IEEE Access
Multidisciplinary | Rapid Review | Open Access Journal

Received August 6, 2019, accepted August 19, 2019, date of publication August 23, 2019, date of current version September 9, 2019.

Digital Object Identifier 10.1109/ACCESS.2019.2937103

A Motor Fault Diagnosis System Based on Cerebellar Model Articulation Controller

PI-YUN CHEN, KUEI-HSIANG CHAO, (Member, IEEE), AND YU-CHENG TSENG
Department of Electrical Engineering, National Chin-Yi University of Technology, Taichung 41170, Taiwan

Corresponding author: Kuei-Hsiang Chao (chaokh@nct.edu.tw)

This work was supported by the Ministry of Science and Technology, Taiwan, under Grant MOST 103-2221-E-167-015-MY3.

ABSTRACT The purpose of this paper is to construct a smart induction motor fault diagnosis system with cerebellar model articulation controller (CMAC). First, we divide induction motor faults in three kinds, rotor mandrel fault, bearing fault and electrical fault. Then, we subdivide them into ten types, in each of which the vibration signal spectra of induction motors were measured and sorted for establishing the individual fault types. From the information on motor faults, we identify representative characteristic frequency spectra for the faults to further establish the correlations between each of the fault types and its corresponding characteristic frequency spectrum as the basis for the development of a motor fault diagnosis system. In this paper, the theoretic basis is CMAC, and the data of vibration signal spectrum measured against the motor faults are used to train the fault diagnosis system. We then conducted fault diagnoses with the data of actual motor run. The test results demonstrated that the proposed induction motor fault diagnosis system is capable of fast algorithm, requires less data to train with, as well as has excellent power of identification.

INDEX TERMS Fault vibration signal, cerebellar model articulation controller (CMAC), characteristic frequency spectrum, motor fault diagnosis.

I. INTRODUCTION

Motors play an arduous role in industries. Due to their high economic benefit and robustness, they are extensively employed in all sorts of production equipment. Thus, not only can the labor of maintenance and cost of repair be significantly saved but the factory productivity will be protected against accidental disruption if it is possible to identify the causes of motor faults and repair them as early as possible by means of monitoring apparatus and an automated diagnosis system when the faults show at an early time. Presently the conditions of motors are all determined by specialists' analysis of the vibration signals that have been taken on the motors with apparatus; the specialists further figure out the causes of such abnormal motor vibrations. The results of determination, however, can be very different because every specialist has different levels of knowledge and experience and may use different analytic methods. Besides, as technologies continuously make breakthrough and develop, production equipment is becoming larger and automated as well as consisted of complicated components, the conventional diagnosing methods cannot be useful any more.

The associate editor coordinating the review of this manuscript and approving it for publication was Seyedali Mirjalili.

There are faults during the operation of automated equipment, of which motor faults are the worst. In general, motors with faults are not just the problem of the mechanical structure of the motors themselves; they sometimes have faults as a result of their operation. Hence, how to accurately discern whether a motor has faults and the causes of such faults is an issue worth investigating. So far, motor faults have been determined by measuring certain signals on the motors using apparatus as data gathered at time of fault for specialists to identify the causes of such faults. Long ago, motor faults were diagnosed by displaying the messages that were measured with apparatus in numeric or waveform, by which results one could easily and quickly know a fault(s) has/have happened. Yet, it needed workers on site to further study those messages based on their experience to identify the types of faults before repair or replacement was made. Such conventional fault diagnosis, however, is liable to lead to incorrect determination of where the fault is, which causes undesired waste of effort and time on service and replacement [1]–[3]. Hence, new diagnosis techniques to locate the positions of system faults is a direction deserving probing. Presently, researchers have put a lot of effort in quest for such techniques [4]–[7]; for instance, an attempt to employ algorithms of artificial intelligence [4] in motor fault diagnoses, which method can

enhance the efficiency of motor fault diagnoses, helping save effort and time. Other researchers applied methods of neural network (NN) [5]–[7] to create fault diagnosis system, which uses the weighting value connecting neurons to do algorithms to, in turn, determine the types of faults. That is a method capable of making faster diagnoses though, it requires a lot of data to learn with [8]–[12]. There are other algorithms used in the study of motor fault diagnoses; examples are the neural-fuzzy [1] and the approximate reasoning [3]. The former is used in a method that does not require a mathematical model built for motors, but simply builds a fault diagnosis system based on the correlations between inputs and outputs; yet, the algorithm it uses takes longer time to arrive at optimal solutions and makes only one single record in data recognition. The latter is used in a diagnosis method that does simple calculations and is easily realized, however, has a drawback of misdiagnosis when the article under diagnosis has differences with insignificant characteristics. The study in [13] can successfully diagnose three motor fault diagnosis types, namely abnormal air-gap eccentricity, bearing failure, and broken rotor bar by using motor stator current power spectrum. Nevertheless, these motor fault diagnoses cannot clearly identify the exact fault position. Hilbert and Wavelet Transforms and Knowledge Extraction methods [14]–[16] using data mining technique have been applied to convert time–frequency plots into frequency–amplitude plots, and then with the genetic algorithm selected the fault characteristics and diagnoses motor fault types. However, it can diagnose only six motor fault types.

An intelligent fault diagnosis of three-phase induction motors using a signal-based method was proposed in [17]. This technique was tested in different situations to demonstrate its effectiveness in fault diagnoses, even when the information about operating modes is limited or difficult to obtain. However, the obtained results proved the efficiency of the proposed method covers not more than the diagnosis of broken bars and bearing failure. Additionally, to accurately diagnose motor faults, such as broken bars, mixed eccentricity, and shaft bearing fault, the characteristic spectra of motor vibration signals and stator current have been obtained in [18]–[23]. However, other motor fault types demonstrating the same fault characteristic spectra still exist, but with different amplitudes, thus resulting in the false detection of a motor fault type during motor fault diagnosis.

Because CMAC has the ability to associate and summarize and has the characteristics of having similar memory stimulated by similarity input signals, the classification of learning materials has a higher accuracy than that of other methods. In addition, the test data, according to its similarity with the specific fault characteristics, can output the most probable type of fault by CMAC automatically, and because of its high anti-noise interference, it has a good robustness in the system fault diagnosis. Moreover, because CMAC uses less memory and has a fast learning speed and fault tolerance, there have been cases of its successful application on the equipment fault diagnosis of photovoltaic power generation systems [24] and power systems [25]. However, it has not yet been applied to motor fault diagnosis. Therefore, this paper presents a smart technique of fault diagnosis built using CMAC. This technique not only allows workers on site to locate the positions of fault in less time, speeding up the service, but also allows the specialists on site to determine the length of period of system downtime based on the messages obtained from the fault diagnosis, thus increasing overall economic benefit.

II. ANALYSIS OF MOTOR FAULT TYPES AND FREQUENCY SPECTRUM CHARACTERISTICS

Ten common motor faults can be roughly divided in the types of rotor mandrel fault, bearing fault and electrical fault [1]–[3]. The causes of rotor mandrel faults include the characteristics of rotor unbalance, rotor bending, rotor misalignment and rotor looseness. When each of these specific faults occurs, a characteristic frequency spectrum for the motor vibration is picked up by the frequency spectrum analyzer, as Table 1 shows. Of the four characteristics, rotor unbalance relates to a characteristic frequency spectrum that occurs at 1 times the frequency of rotor speed, represented by $1X$, the same applies to other frequency spectra. With rotor bending, the picked-up frequency spectra are at $1X$, $2X$ and $3X$, where a highest peak appears at $1X$, with peaks of frequency spectrum decreasing from $1X$ to $3X$. As with rotor misalignment, the characteristic frequency spectrum for $2X$ has the highest peak, among those for $1X$, $3X$ and $4X$, where that for $4X$ has the lowest peak. As to the frequency spectra exhibited with rotor looseness, while a greater peak of frequency spectrum appears at $1X$, there are other multiple frequencies like $0.5X$, $1.5X$, $2X$, $2.5X$ and $3X$, of which the integer multiple frequency spectra have more obvious peaks that show a sign of decreasing with the integer.

Faults in the motor's bearing assembly are oil-film bearing fault and ball bearing fault; this paper focuses more on the latter. In a motor with a bearing structure being of ball bearing, a fault can fall in any of the following: inner ring damage, outer ring damage and ball damage, the characteristic frequency spectra of which are listed in Table 1. When an inner ring damage occurs, the frequency clusters that arise can be expressed by [4], [5]

$$m \times f_{in} \pm n \times f_{\omega} \quad m = 1, 2, 3, \ldots; \; n = 0, 1, 2, \ldots \tag{1}$$

$$f_{in} = \frac{1}{2}(f_{\omega} M + \frac{df_{\omega} M}{D} \cos\alpha) \tag{2}$$

where f_{in} is the frequency noticed when the ball passes the starting point of the inner ring, f_{ω} the bearing rotational frequency, M the number of balls, d the ball diameter, D the bearing node-path, and α the contact angle.

The frequency spectra for the faults due to outer ring damage are, as can be found in Table 1, similar to those from inner ring damage; both appear in the form of frequency cluster. Thus, the positions of frequency clusters for outer ring

TABLE 1. Types of motor faults and corresponding characteristic frequency spectra.

Position of fault	Fault type	Characteristic frequency spectrum
Motor rotor mandrel fault	Rotor unbalance	The highest peak appears at $1X$, with few components of other harmonic frequency.
	Rotor bending	Frequency spectra appear at $1X$, $2X$ and $3X$, decreasing in that order.
	Rotor misalignment	The frequency spectrum at $2X$ has higher value, with those at $1X$ and $3X$ a little lower than at $2X$; the frequency spectrum at $4X$ also shows a value.
	Rotor looseness	The frequency spectra at $1X$, $2X$ and $3X$ have outstanding value, which decrease in that order; there are also fractional frequencies.
Motor bearing fault	Inner ring damage	Frequency cluster appears in the form of $mf_{in} \pm nf_{\omega} (m = 1, 2, 3, \ldots$; $n = 0, 1, 2, \ldots)$.
	Outer ring damage	Frequency cluster appears in the form of $mf_{out} \pm nf_{cage} (m = 1, 2, 3, \ldots$; $n = 0, 1, 2, \ldots)$.
	Ball damage	Frequency cluster appears in the form of $mf_{roller} \pm nf_{cage}$ $(m = 1, 2, 3, \ldots$; $n = 0, 1, 2, \ldots)$.
Motor electrical fault	Air gap unbalance	Frequency clusters emerge at $1X \pm nf_p$ and $2f_L \pm nf_p$ $(n = 1, 2, 3, \ldots)$.
	Rotor bar break	Frequency spectra at $1X$ and $2X$ as well as in the form of frequency cluster at $f_b + nN_r$ $(n = 1, 2, 3, \ldots)$.
	Phase unbalance	The frequency spectrum is obvious at $6f_L$; another appears at $1X$.

damage can also be expressed by [4], [5]

$$m \times f_{out} \pm n \times f_{cage} \quad m = 1, 2, 3, \ldots; \; n = 0, 1, 2, \ldots \tag{3}$$

$$f_{out} = \frac{1}{2}(f_{\omega} M - \frac{df_{\omega} M}{D} \cos\alpha) \tag{4}$$

$$f_{cage} = \frac{1}{2}(f_{\omega} - \frac{df_{\omega}}{D} \cos\alpha) \tag{5}$$

where f_{out} stands for the frequency when the ball passes the starting point of outer ring, and f_{cage} the revolution frequency of the ball.

The positions of the characteristic frequency spectrum due to ball damage can be expressed, via the mathematical model, by [1], [2]

$$m \times f_{roller} \pm n \times f_{cage} \quad m = 1, 2, 3, \ldots; \; n = 0, 1, 2, \ldots \tag{6}$$

$$f_{roller} = \frac{1}{2}(\frac{Df_{\omega}}{d} - \frac{df_{\omega}}{D} \cos^2\alpha) \tag{7}$$

In (6) and (7), f_{roller} stands for the frequency when the ball passes outer ring or inner ring.

In addition, if the electromagnetic force is unevenly distributed during motor run, that would cause electrical fault, where the electromagnetic force is generated when there is current and gone immediately when the power is disconnected. Unevenly distribution of electromagnetic force is caused by the factors of air gap unbalance, rotor bar break, phase unbalance, and so on. Characteristic frequency spectra in such cases are shown in Table 1. The fault frequency spectra in the case of air gap unbalance stand out at $1X$ (i.e., equal to the frequency of rotation) and $2f_L$, and each is accompanied by a sideband frequency whose frequency distance is f_p. f_L is the frequency of power source, and f_p is the pole passing frequency, expressed as [1], [2]

$$f_p = P \times f_s \tag{8}$$

In (8), P stands for the number of pole of rotor, f_s for slip frequency which can be expressed by

$$f_s = \frac{N_s - N_r}{60} \tag{9}$$

where N_r is rotor speed, and N_s is synchronous speed, mathematically expressed by

$$N_s = \frac{120 f_L}{P} \tag{10}$$

The characteristic frequency spectra for the fault in the case of rotor bar break show value at $1X$ and $2X$, while other frequency spectra also appear at the main frequency of f_b and at a sideband frequency whose frequency distance is N_r. f_b stands for rotor bar passing frequency, mathematically expressed by

$$f_b = \frac{B - N_r}{60} \tag{11}$$

In (11), B stands for the number of rotor bars. As to the characteristic frequency spectrum in the case of phase unbalance fault, the frequency spectrum at $6f_L$ (i.e., 6 times the frequency of power source) has a higher peak, another is seen on the 1 times rotation speed frequency.

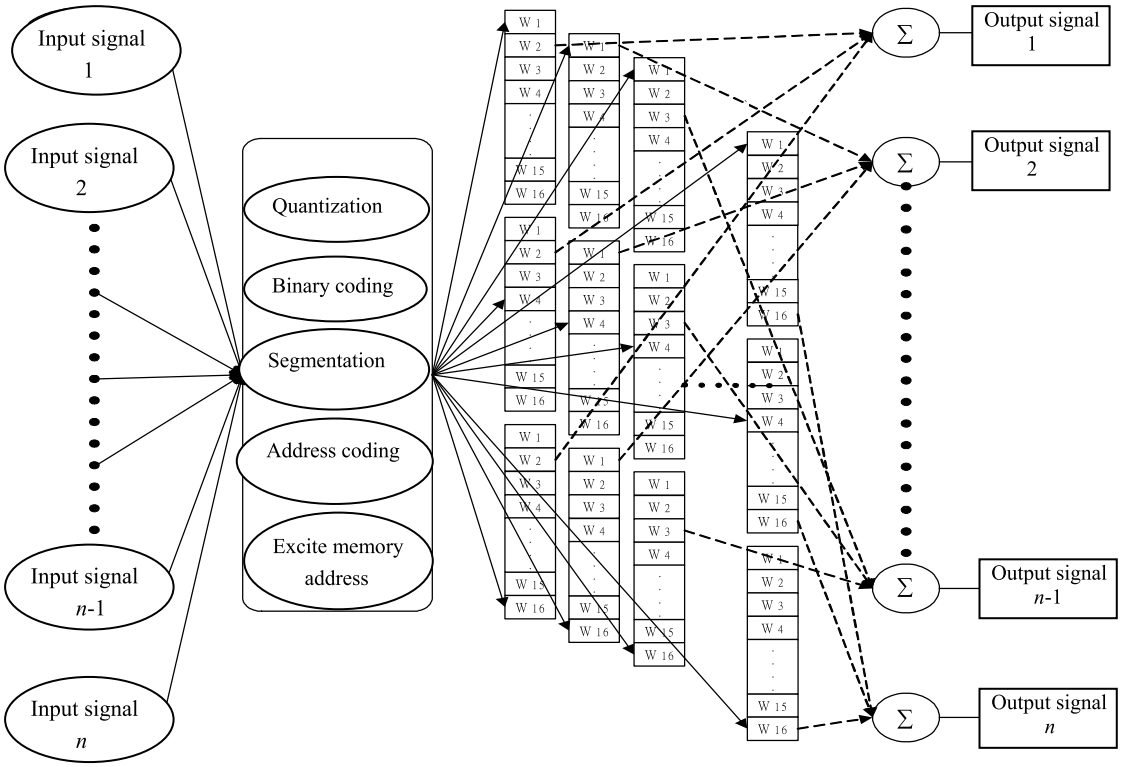

FIGURE 1. CMAC framework.

III. CEREBELLAR MODEL ARTICULATION CONTROLLER

Cerebellar model articulation controller (CMAC), was first proposed by Ablus in 1970 [26], who hoped to imitate the neural structure of human cerebellum to achieve the feature of fast learning and prompt response. A CMAC activates related memories based on the input signals received in different sizes, where similar input signals activate similar memories. Instead of any algorithmic framework of multiple layers of memories in the entire neural network, memory cells are used to store mapping between input signals and output signals. Though the capacity of the memories may be huge, each input signal can excite only a small group of memories and not all the memories are used. That resembles the structure of human cerebellum, which has a huge capacity of memory but uses only a small portion of them for any specific input signal. In a memory structure of cerebellar model articulation controller as Fig. 1 shows, each memory address stores a weighting value, w. When a signal is inputted, it is quantized, coded, and a combination of addresses is excited to a set of memory addresses. With the weighting value of such excited set of memory addresses summed up, the output can be mapped by the input signals of this set. Compare such output value with the ideal one for the value of difference, and evenly distribute the difference to this excited set of memory addresses as tuning to complete the training of a record of data. Like other neural networks, CMAC comprises a training phase and a diagnostic recognition phase [27]. We will begin by elaborating on the training phase. The steps of a CMAC training are as Fig. 2 shows.

A. QUANTIZATION

In order to successfully code the analog signals inputted, it is necessary to begin with signal quantization. In concept, this quantization is in fact the same as what an average analog-to-digital IC does. The conversion executed can be expressed by (12).

$$Q_x(x) = ceil\left((x - x_{\min}) / \left[(x_{\max} - x_{\min}) / Q_{\max}\right]\right) \quad (12)$$

where, x is the input to be quantized, $Q_{\max}$ the maximum level of quantization, ceil($\cdot$) the command of choosing a greatest integer, and $[x_{\min}, x_{\max}]$ the minimum and maximum of the training samples. Divide each input into several equally spaced quantized levels between the maximum and the minimum. The quantized levels of higher definition result in finer quantization coding, but require larger memory spaces [24].

B. CODING THE EXCITED ADDRESSES

The resultant values from quantization will be coded. Assume a set of input signals is quantized into the levels of (5, 10, 8, 12). Make binary coding of such levels into 0101_b, 1010_b, 1000_b, 1100_b, which are combined into a 16-bit code, 1100100010100101_b.

Segment the above mentioned resultant codes in groups of, say, 3 bits. Thus, there will be six groups, which are coded in the order from the least significant bit (LSB) to the most significant bit (MSB), and excite six addresses, namely, $a_1 = 101_b = 5$, $a_2 = 100_b = 4$, $a_3 = 010_b = 2$, $a_4 = 100_b = 4$, $a_5 = 100_b = 4$ and $a_6 = 001_b = 1$, in the same order.

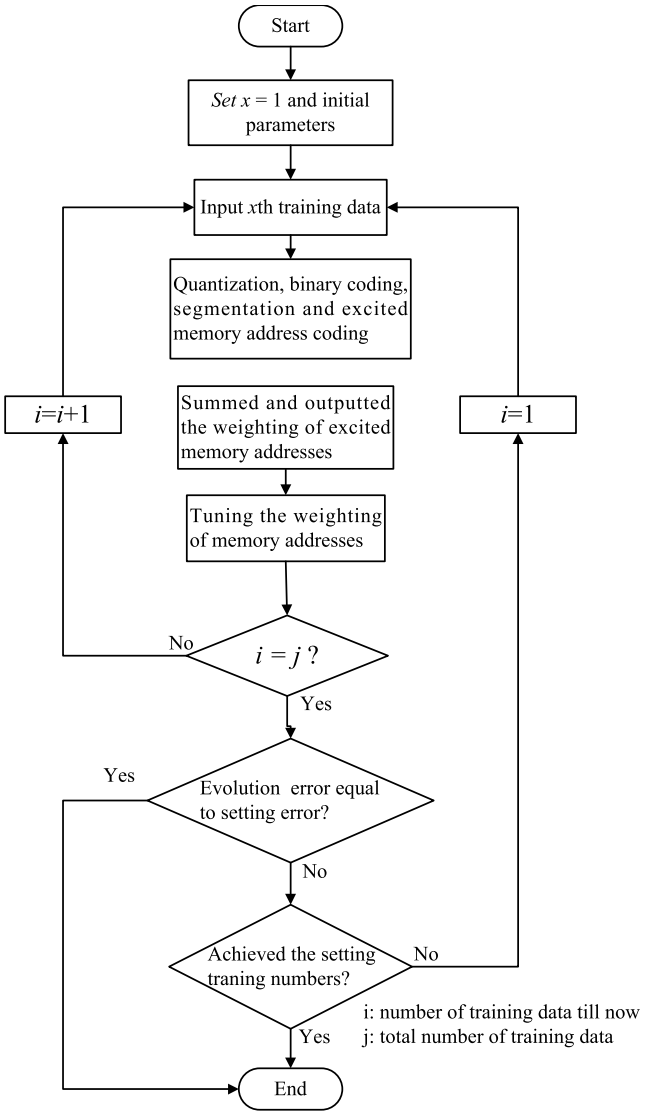

FIGURE 2. Flow chart of CMAC training.

Let these decimal values correspond to memory spaces. Assume the initial weights of the memories are all 0; then, the sum of the memory weights in the first excitement is 0.

C. WEIGHT ADJUSTMENT

Assume the sum output for a fault type has a weight at 1; that means this datum is classified as this fault type. Whilst, when the weight for a sum of memories is not 1, it should be adjusted. Weight adjustments are as (13) shows [25], [28].

$$w_{new}^{ai} = w_{old}^{ai} + \beta \frac{Y_d - Y}{A^*} \tag{13}$$

where a_i is the address of an excited memory, and β the training constant, whose value is somewhere between 0 and 1. Assume any fault type has only one set of training samples. Then, we can just let β be 1. Where there are more than one sample data, β is normally a little smaller than 1. Y_d is the target value (set at 1 herein), Y is the actual output value, and A^* is the quantity of excited memory addresses, implying that the weights to be trained are evenly distributed to the memory addresses.

D. FAULT TOLERANCE

The CMAC proposed herein has good interference immunity. Take the 16-bit coding in Section III. B for example, if the original code ($1100\underline{1}100010100101_b$) should change to ($1101\underline{1}100010100101_b$) due to interference, then the excited address (a_6, a_5, a_4, a_3, a_2, a_1) after coding will change from (1, 4, 4, 2, 4, 5) to (1, 5, 4, 2, 4, 5), where an error arises only at a_5, with all the rest normally outputted. That demonstrates the capability of fault tolerance. Accuracy can be further increased if we further increase the number of groups, distributing the storage to more addresses and thus helping mitigate the influence of the fault detected in adjacent bits on the output.

E. CONVERGENCE

The framework of CMAC includes a training method with monitoring and its convergence has been demonstrated in documents [29]. As it uses coding, the CMAC proposed herein is able to significantly reduce the use of memories. Also, because no other coding principles are used to compress the rate of memory use, the weights of memories do not collide in the course of training, which helps ensure the convergence of training.

F. ASSESSMENT OF LEARNING EFFECT

When the ith ($i = 1, 2, 3, \ldots$) layer inside a memory is excited, the weights in the memory addresses are summed up. If the output sum approximates or is equal to 1, that means the datum falls in the ith output type. If the count of data in the ith output type is d, the learning effect, E, is evaluated by an index

$$E = \sum_{i=1}^{d} (y_i - 1)^2 \tag{14}$$

To determine whether the learning is complete, check if $E < \varepsilon$ is met for assessing the learning effect, where ε is the parameter for convergence. When $E < \varepsilon$ is satisfied, the CMAC training can be stopped.

IV. MEASUREMENT OF INDUCTION MOTOR FAULT SIGNALS

The framework of the motor fault diagnosis system probed herein adopts the CMAC, and includes tests, whereby the excellent performance of CMAC's application in fault diagnoses is compared. In the test, a frequency spectrum analyzer is used to measure motor vibration signals, which will be subjected to Fast Fourier Transform (FFT) to become frequency domain signals for extracting the data necessary for fault diagnosis. Then, based on the data of motor fault detection in the tests, the relationship between motor fault categories and characteristics is established as the basis for the data for training by CMAC fault diagnosis.

TABLE 2. Codes for motor fault types.

Motor fault type	Code	Fault
Motor rotor fault	MF_{01}	Rotor unbalance
	MF_{02}	Rotor bending
	MF_{03}	Rotor misalignment
	MF_{04}	Rotor looseness
Motor bearing fault	MF_{05}	Inner ring damage
	MF_{06}	Outer ring damage
	MF_{07}	Ball damage
Motor electrical fault	MF_{08}	Air gap unbalance
	MF_{09}	Rotor bar break
	MF_{10}	Phase unbalance

TABLE 3. Codes for characteristics of motor faults.

Motor fault type	Code	Characteristic
Motor rotor fault	C_{01}	Frequency at $0.5X$ rotation speed.
	C_{02}	Frequency at $1X$ rotation speed.
	C_{03}	Frequency at $1.5X$ rotation speed.
	C_{04}	Frequency at $2X$ rotation speed.
	C_{05}	Frequency at $2.5X$ rotation speed.
	C_{06}	Frequency at $3X$ rotation speed.
	C_{07}	Frequency at $4X$ rotation speed.
	C_{08}	Frequency lower than $0.5X$ rotation speed.
	C_{09}	Axial vibration greater than radial vibration.
	C_{10}	The frequency at $2X$ rotation speed higher than that at $1X$ rotation speed.
Motor bearing damage	C_{11}	Characteristic frequency of inner ring damage.
	C_{12}	Characteristic frequency of outer ring damage.
	C_{13}	Characteristic frequency of ball damage.
Motor electrical fault	C_{14}	Frequency at twice the power.

A. ESTABLISMMENT OF MOTOR FAULT TYPE-CHARACTERISTICS RELATIONSHIP

Motor faults are diagnosed for types based on the fault types and their corresponding characteristic frequency spectrum peaks that are given in Table 1. As such, to be able to promptly diagnose a fault type when a motor fault occurs, it is necessary to establish in advance the relationship between motor fault types and their corresponding characteristics. We sorted the causes of motor faults into ten types and give them codes in Table 2. The classification of the motor fault categories used in this paper and the distribution of the characteristic frequency spectrum of vibration signals generated by the different fault categories are classified according to references [1]–[3]. Therefore, MF_{01} to MF_{10} in Table 2 represent the code names of various fault categories of the motor, and C_{01} to C_{16} in Table 3 represent the code names of the spectral values at the respective frequencies when the motor has different faults. The spectral values of the specific frequencies under different faults will be different or even non-existent. Therefore, based on the existence of the values and the values of C_{01} to C_{16}, the MF_{01} to MF_{10} fault categories can be accurately determined with the CMAC method proposed in the paper. In the Table 2, MF_{01} to MF_{04} represent those of motor rotor faults, MF_{05} to MF_{07} represent those of motor bearing faults, and MF_{08} to MF_{10} represent those of motor electrical faults. In the Table 3, C_{01} to C_{10} represent the characteristic frequency spectra of motor rotor faults, C_{11} to C_{13} represent those of motor bearing damages, and C_{14} to C_{16} represent those of motor electrical faults.

B. MEASURED EQUIPMENT OF CHARACTERISTIC FREQUENCY SPECTRUM

A vibration analyzer, having sensors, transforms the physical quantities of mechanical vibration (displacement, speed, acceleration) into voltage, electric charges and current signals; the signals are then amplified by amplifiers and undergo frequency spectrum analysis by the Fast Fourier Transform, FFT. The apparatus comprises a vibration meter, a spectrum analyzer, a balance instrument and a vibration transducer, and transforms, with FFT frequency spectrum analysis, complex time domain waveforms into frequency spectra in order to better understand the causes of vibrations. The spectra analyzer, as shown in Fig. 3 with its related ancillary devices used herein, uses the frequency of 60Hz (1.8k=1,800 RPM) as the $1X$ frequency benchmark and is capable of displaying frequency spectra of $0.5X$, $1X$, $1.5X$,$2X$, $2.5X$, $3X$, $3.5X$, $4X$, $4.5X$, $5X$, $5.5X$, $6X$ and $6.5X$ in the screen [30].

C. TEST OF NORMAL MOTOR SIGNALS

We began with a brand new, normal motor that is within tolerance as the benchmark for frequency spectrum tests, allowing comparison of the vibration frequency spectra measured in ten types of motor faults. The motor was powered by the 60Hz grid, which was equivalent to the motor's synchronous speed at 1.8k RPM. Fig. 4 shows the vibration frequency spectra measured on the motor. It is observed that the frequency of $0.5X$ appears at 0.9k in the X-axis, that of $1X$ at 1.8k, that of $2X$ at 3.6k; the same applies to the rest. It becomes obvious from the spectrum that in normal motor run, its vibration

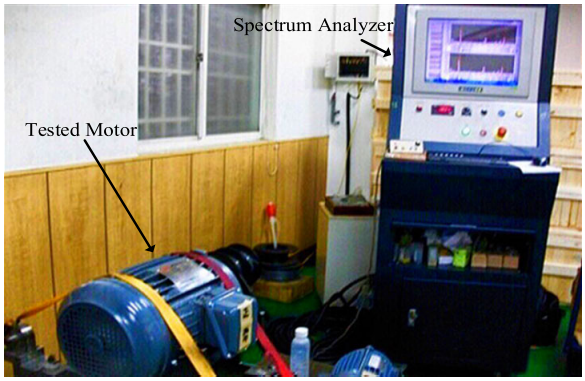

FIGURE 3. Photo of the spectrum analyzer and accompanying measuring devices.

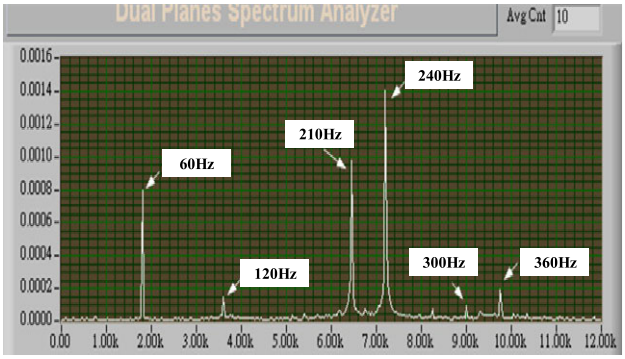

FIGURE 4. Spectrum of vibration on a normal motor.

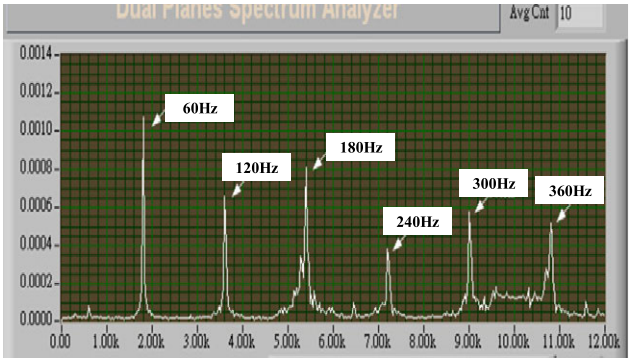

FIGURE 5. Spectrum of vibration on a rotor bending.

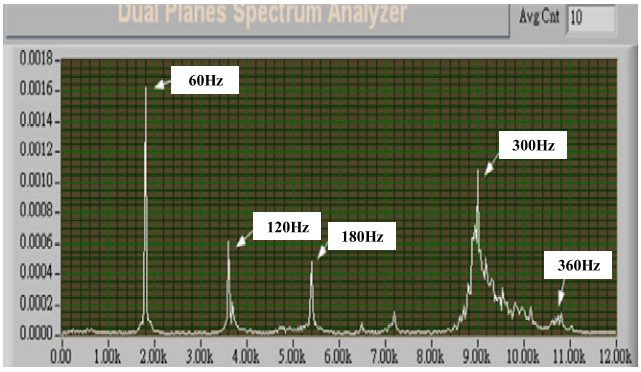

FIGURE 6. Spectrum of vibration on inner ring damage.

frequencies exhibit outstanding signals at $1X$, $2X$, $3.5X$ and $4X$. Comparing these with the ten fault types in Table 1, we discovered that this motor had minor rotor unbalance, rotor bending, phase unbalance and looseness, except that these were all within the range of tolerance [30].

D. TEST OF FAULT MOTOR SIGNALS

Due to limitation of an article, only test results of the bending signals in motor rotor mandrel fault, inner ring damage signals in motor bearing fault and rotor bar break signals in motor electrical faults are shown herein.

1) Test of rotor bending signals in motor rotor mandrel fault: The fault type of "rotor bending" generally gives rise to apparent axial vibration, and on the same rotational axis, the axial vibrations are 180 degree out of phase. If the bent portion is near the middle of the shaft, then the frequency at $1X$ will be the main frequency. However, if the bent portion is near the shaft coupling, the vibration is primarily the frequency at $2X$. Fig. 6 shows its vibration spectrum, where obviously the value of $1X$, $2X$, $3X$, $4X$, $5X$, $5.5X$ and $6X$ frequencies stand out. From Fig. 5 it can be observed that the value of the main frequency at $1X$ rises, so does that at $2X$. Compared with the ten fault types in the Table 1, it is certain that this is of the "rotor bending" type, which also may lead to phase unbalance at $4X$ frequency and would cause axial vibration at $5X$ frequency and radial vibration at $6X$ frequency [30].
2) Test of inner ring damage signals in motor bearing fault: The fault type of "inner ring damage" is characterized by beginning to show natural frequency of bearing ball elements, mf_{in}, possible natural frequency of bearing structure, $2f_{in}$, and the frequency of ball passing the starting point of inner ring on both ends, f_{ω}, all due to the bearing damage. When the wearing increases, more damage frequencies and harmonics and sideband frequencies of natural frequencies grow with it. The $1f_{in}$ frequency could be affected, too, such that its amplitude becomes unusually large. As Fig. 6 shows, obviously in the spectrum, the frequencies at $1X$, $2X$, $3X$, $5X$, and $6X$ stand out. Compared with the ten fault types in Table 1, we can be more certain that this is an "inner ring damage", which is also accompanied by ball spin-caused axial vibration at $5X$ frequency and radial vibration at $6X$ frequency, leading to the motor's structural vibration [30]. The dominant natural frequency spectrum is in Fig. 6, as for sideband frequencies of the natural frequencies due to damage is not enough, so it is not obvious.
3) Test of rotor bar break signals in motor electrical fault: The fault type of "rotor bar break" features the structural natural frequencies between the motor stator coils and the rotor that are caused by uneven distribution of electromagnetic force during motor run.

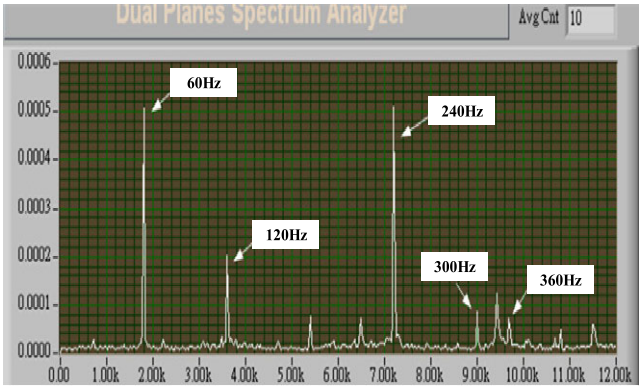

FIGURE 7. Spectrum of vibration signals on rotor bar break.

Electromagnetic force is created when the motor is energized and disappears on the instant the power is disconnected. Besides the frequency spectra at $1X$ and $2X$ frequencies showing numbers, the frequency spectrum of main frequency at f_b and the sideband frequency with sideband frequency distance at N_r are also seen. Fig. 7 shows that in spectrum obviously the frequency spectra at $1X$, $2X$, $4X$ and $5X$ stand out. When comparing with the ten fault types in Table 1, we can be more certain that this is of the ''rotor bar break'' type, where vibrations also occur due to phase unbalance during ball spin, which causes $4X$ frequency, and axial vibration a $5X$ and harmonics at $5.5X$ frequency [30].

V. MOTOR FAULT DIAGNOSIS TEST RESULTS

A. TRAINING PROCESS OF CMAC MODE

The training process of CMAC model proposed herein is as Fig. 2 shows. To begin with, for training data of the CMAC model, use ten vibration frequency spectrum signals (a total of 100 data) of each of the ten fault types, which are rotor unbalance, rotor bending, rotor misalignment, rotor looseness, inner ring damage, outer ring damage, ball damage, air gap unbalance, rotor bar break and phase unbalance that happened to the induction motor measured in Section IV. Establish the parameters for CMAC model, including quantity of input signal, size of quantization levels, number of bits for segmenting excited memory address, and types of output signal. With characteristic frequency spectrums captured when the induction motor has a different fault type as the training data samples in the CMAC model, quantize these samples, subject them to binary coding, segment the excited memory addresses and excite memory addresses, followed by summing up the weightings in the excited memory addresses to determine the output value of each fault type. Then compare the output value with the target value ($y_d = 1$) to adjust the weighting in the excited memory addresses. Check and ensure all the data samples of characteristic frequency spectrums for the fault types of the induction motor have undergone training by loading each and every of them in the CMAC model for training. When the training is finished, assess the learning effect. If for learning effect, $E <$ rate of convergence, ε, holds, save the weighting in the excited memory addresses, completing the CMAC model training.

TABLE 4. Related parameters to CMAC.

Related parameter	
Number of inputs	4
Number of outputs	10
Number of quantification levels	16
Number of bits per group	4
Number of groups	4
Learning constant (β)	0.9
Number of training session	5

The algorithmic process is described as follows:

1) Gather the characteristic frequency spectrums measured on the different fault types of the induction motor.
2) Input these characteristic frequency spectrums in the CMAC system for training.
3) Subject these characteristic frequency spectrums to quantization and binary coding, segment the excited memory addresses and excite memory addresses, and tuning the weighting in the excited memory addresses.
4) Sort all the characteristic frequency spectrums for induction motor fault types to complete the training of CMAC induction motor fault diagnosis system.

B. DIAGNOSIS PROCESS OF CMAC MODE

The process of fault diagnosis for induction motor by CMAC proposed herein is as follows:

Step1: Initialize the related parameters, as Table 4 shows. Quantize the input signals, which are the characteristic frequency spectra for the 16 vibration signals during motor faults listed in Table 3.

Step2: Convert the quantized value by binary coding and recombine them. Group the combined codes. Herein, 4 bits of code are a group; there are four groups.

Step3: Locate the memory addresses corresponded by the grouped coding; sum up the weighting in such memories. The memory space used herein is of 10 layers; hence, 10 layers of memory of a same address are excited, resulting in 10 outputs.

Step4: Determine the weighting of the 10 outputs. When the weighting is larger and closer to 1, that implies a higher probability of such fault occurring.

C. DIAGNOSTIC RESULTS

The CMAC algorithm and identification process in Fig. 2 were employed, and the ten fault types often seen on induction motors listed in Table 2 and the characteristic frequency spectra for 16 types of faults in Table 3 were taken as the basis. A total of 100 vibration signal frequency spectra measured in the ten motor fault types were used as data of learning

TABLE 5. 20 Data to be identified for motor fault types.

Sample No.	Fault Characte-ristics																Known fault type
	C_{01}	C_{02}	C_{03}	C_{04}	C_{05}	C_{06}	C_{07}	C_{08}	C_{09}	C_{10}	C_{11}	C_{12}	C_{13}	C_{14}	C_{15}	C_{16}	
1	0.0133	0.5862	0.0373	0.0348	0.1250	0.0659	0.0228	0.1032	0.0569	0.1092	0.0228	0.0634	0.0473	0.0555	0.0972	0.0459	MF_{01}
2	0.0248	0.6901	0.0842	0.0856	0.0442	0.0451	0.1022	0.0963	0.1072	0.0193	0.0123	0.0836	0.0193	0.0859	0.0687	0.0257	MF_{01}
3	0.0482	0.3074	0.0823	0.7187	0.0003	0.5388	0.0467	0.0278	0.0000	0.0278	0.6387	0.5732	0.0046	0.0643	0.0123	0.2947	MF_{02}
4	0.0228	0.2948	0.0056	0.6364	0.0653	0.6084	0.0133	0.0193	0.0298	0.0379	0.5781	0.5342	0.0538	0.0000	0.0005	0.2795	MF_{02}
5	0.0486	0.2348	0.0099	0.5176	0.0534	0.6646	0.1474	0.0524	0.0022	0.8746	0.0564	0.0478	0.0244	0.0228	0.0288	0.0004	MF_{03}
6	0.0476	0.1366	0.0871	0.3874	0.0467	0.5571	0.1647	0.0293	0.0436	0.5000	0.0000	0.0379	0.0389	0.0123	0.0921	0.0055	MF_{03}
7	0.9912	0.2783	0.7712	0.2555	0.6035	0.2098	0.0133	0.0638	0.0056	0.0289	0.0823	0.0817	0.0538	0.0459	0.1250	0.0365	MF_{04}
8	0.7721	0.3693	1.0000	0.3500	0.7845	0.1843	0.0038	0.0964	0.1171	0.0047	0.0000	0.0412	0.0003	0.1250	0.0244	0.0961	MF_{04}
9	0.0891	0.6148	0.0369	0.3162	0.0119	0.3125	0.0629	0.3800	0.0467	0.0065	0.5771	0.0003	0.0004	0.0022	0.2781	0.0123	MF_{05}
10	0.0478	0.5208	0.0643	0.3884	0.0923	0.4186	0.0003	0.3579	0.0133	0.0531	0.5725	0.0544	0.0097	0.0618	0.3659	0.0027	MF_{05}
11	0.0193	0.2878	0.0399	0.3220	0.1250	0.6705	0.0486	0.2936	0.0175	0.0289	0.0467	0.8463	0.0228	0.0763	0.2796	0.1250	MF_{06}
12	0.0008	0.3508	0.0412	0.4820	0.0891	0.6971	0.0000	0.1483	0.0842	0.0119	0.0133	0.7419	0.0123	0.0261	0.4531	0.0544	MF_{06}
13	0.0369	0.4284	0.1022	0.1931	0.0569	0.0041	0.0008	0.1358	0.0003	0.0625	0.0005	0.0133	0.5213	0.0003	0.6777	0.0055	MF_{07}
14	0.0007	0.1752	0.0923	0.2466	0.0477	0.0598	0.0000	0.2468	0.1250	0.0007	0.0056	0.0248	0.7006	0.0134	1.0000	0.0004	MF_{07}
15	0.1250	0.3848	0.0329	0.1848	0.0005	0.0377	0.0817	0.0379	0.0467	0.0389	0.0054	0.0881	0.0027	0.6914	0.1841	0.4096	MF_{08}
16	0.0335	0.3982	0.0482	0.1594	0.0486	0.0003	0.0097	0.0000	0.0133	0.0008	0.1250	0.0712	0.0828	0.5348	0.1262	0.5414	MF_{08}
17	0.0329	1.0000	0.0618	0.8096	0.0278	0.0467	0.0003	0.0974	0.0152	0.0067	0.2864	0.0027	0.0379	0.0735	0.0097	0.0288	MF_{09}
18	0.0293	0.8843	0.0311	0.9017	0.1095	0.0133	0.0099	0.1171	0.0471	0.0163	0.2564	0.0289	0.0478	0.0311	0.0412	0.0716	MF_{09}
19	0.0008	0.1732	0.0665	0.0583	0.0823	0.0000	0.9809	0.0492	0.0619	0.0152	0.0248	0.0633	0.0065	0.1250	0.0006	0.0046	MF_{10}
20	0.0389	0.2121	0.0261	0.0005	0.0046	0.0379	0.8396	0.0000	0.0049	0.0832	0.0087	0.0394	0.0231	0.0004	0.0677	0.0436	MF_{10}

in the training, to further establish an induction motor fault diagnosis system by CMAC. With such diagnosis system built with CMAC, we put the 20 data of characteristic frequency spectra measured on the motor fault signals listed in Table 5 to the test by the fault diagnosis process in Section V. *B*. It can be observed from Table 6 that the fault category of each fault test data can be correctly identified. Taking the 10th test data in Table 5 for example, the known fault category is MF_{05} (inner ring damage), and from the result of identification in Table 6 its weighting value of 1.0011 in the fault category MF_{05} is the highest among all the fault categories. Therefore it can be judged to be in the MF_{05} fault category. The weighting value of 0.5451 in the fault category MF_{04} (rotor looseness) is the lowest, so its probability of being in the MF_{04} fault category is the lowest. The test results are as Table 6 shows, which reveal that the proposed motor fault diagnostic technique was capable of 100% accurately identifying the fault types of these data, which verified the effectiveness of the proposed motor fault diagnostic system. The fault diagnosis accuracy of this paper is defined as n/N, where N is the total number of test data and n is the correct number of fault diagnosis.

To further demonstrate the effectiveness of the proposed motor fault diagnosis based on CMAC, we compared the diagnostic results by this method and by other neural network systems [7] in Table 7. In addition, other than a comparison with the multilayer perceptron (MLP) method on the fault diagnosis performance, a comparison with the fuzzy neural network (FNN) [1] and the extension theory (ET) [3] is added to highlight the superiority of the proposed fault diagnosis method. The results of the comparison are also shown in Table 7. The table reveals that our proposed method has less training time and higher accuracy than conventional multilayer perceptron (MLP) method with different perceptrons, fuzzy neural network and extension theory, demonstrating its excellence. The parameters of the FNN [1] and ET [3] are based on the best parameters chosen by the authors, so it is fair to make a comparison.

When the same category of faults occurs to the same type of motors with different capacities, the characteristic frequency spectrum of vibration signals generated have the same location, and only the characteristic frequency spectral values will be different. In addition, because CMAC has a training process, and the training data is the characteristic frequency spectrum of vibration signals extracted from the different fault categories of the motor, the proposed fault diagnosis method can be applied to motors with different capacities.

In addition, since the induction motor has the same electrical characteristics of Brushless DC (BLDC) motor, the proposed method is also applicable to the diagnosis of an electrical fault in BLDC motor. However, because the mechanical structure of the two is not the same, the proposed method does not apply to the fault diagnosis of BLDC motor under a mechanical failure. That being said, if the characteristic frequency spectrum of vibration signals of BLDC motor is reanalyzed under various mechanical failures, and if it is used as training data for CMAC, then the proposed method can

TABLE 6. Results of motor fault diagnosis.

Sample	Output weighting for various fault type										Type identified
	MF_{01}	MF_{02}	MF_{03}	MF_{04}	MF_{05}	MF_{06}	MF_{07}	MF_{08}	MF_{09}	MF_{10}	
1	1.0009	0.6692	0.7249	0.7285	0.8012	0.7163	0.7287	0.7155	0.8058	0.8460	MF_{01}
2	1.0005	0.7087	0.7331	0.7380	0.8129	0.7536	0.6966	0.7554	0.7495	0.8586	MF_{01}
3	0.6711	1.0021	0.6093	0.6288	0.7291	0.7068	0.6209	0.6726	0.6528	0.7057	MF_{02}
4	0.6776	1.0019	0.6562	0.5754	0.6700	0.7544	0.5347	0.5458	0.6913	0.6379	MF_{02}
5	0.7212	0.7062	1.0016	0.6651	0.6398	0.7528	0.6469	0.5847	0.6533	0.6993	MF_{03}
6	0.7676	0.6098	1.0014	0.6644	0.6879	0.6189	0.6021	0.5964	0.6748	0.7611	MF_{03}
7	0.6149	0.5807	0.5067	1.0010	0.6428	0.6119	0.5434	0.6160	0.5065	0.5543	MF_{04}
8	0.6789	0.5523	0.5376	1.0014	0.5969	0.5769	0.4939	0.6551	0.5753	0.5370	MF_{04}
9	0.7315	0.6958	0.6282	0.6173	1.0014	0.8144	0.6571	0.6450	0.7340	0.6198	MF_{05}
10	0.6821	0.7111	0.6578	0.5451	1.0011	0.7839	0.6658	0.6593	0.6982	0.6311	MF_{05}
11	0.5920	0.6981	0.5798	0.5962	0.7015	1.0010	0.5443	0.5980	0.4943	0.5330	MF_{06}
12	0.6938	0.7694	0.6791	0.5659	0.7410	1.0008	0.7048	0.6835	0.6696	0.6196	MF_{06}
13	0.8955	0.6594	0.6578	0.6999	0.8124	0.7994	1.0007	0.7599	0.7986	0.7144	MF_{07}
14	0.7637	0.5907	0.6327	0.6290	0.8101	0.7651	1.0004	0.7927	0.8264	0.7089	MF_{07}
15	0.7300	0.6232	0.5760	0.6630	0.6502	0.7161	0.7615	1.0004	0.6654	0.6686	MF_{08}
16	0.7236	0.7347	0.6506	0.6260	0.6480	0.6421	0.7459	0.9997	0.6937	0.6612	MF_{08}
17	0.8816	0.8019	0.7057	0.6344	0.8101	0.7287	0.7350	0.7510	1.0000	0.7111	MF_{09}
18	0.8374	0.7202	0.7125	0.6921	0.7583	0.6944	0.7509	0.6703	0.9997	0.7306	MF_{09}
19	0.8490	0.6988	0.7751	0.6783	0.6726	0.6164	0.6890	0.7630	0.7578	0.9997	MF_{10}
20	0.9607	0.6997	0.8402	0.7211	0.8384	0.7559	0.7876	0.7493	0.8144	0.9995	MF_{10}

TABLE 7. Accuracy comparison between CMAC and MLP neural network methods.

Method	Learning epochs	Learning accuracy	Fault diagnosis accuracy
CMAC	8	100%	100%
MLP (4-7-10) [7]	1,063	90.84%	93.33%
MLP (4-8-10) [7]	1,386	85.68%	90%
MLP (4-9-10) [7]	1,075	96.64%	93.33%
FNN [1]	1,205	97.1%	94.5%
ET [3]	0	100%	97.3%

also be applied to the diagnosis of various types of faults in BLDC motor.

VI. CONCLUSIONS

This paper constructs a motor fault diagnosis model with the algorithm of CMAC, which is capable of nonlinear mapping. Also CMAC has good learning effect and the ability of associative memory and induction. Therefore, it can result in ideal outputs without precise mathematic models or related specialized knowledge. Also, having the feature of exciting similar memory addresses based on similar input signals, CMAC includes the tuning of weighting in the excited memory addresses during the course of training. Thus, it takes less time for training. The fault diagnosis system quantifies and segments the input signals, hence the fault tolerant ability of the motor fault diagnosis is enhanced. Last, the actual diagnostic results demonstrated that the proposed motor fault diagnosis system has 100% accuracy in identification. Furthermore, since the smart motor fault diagnosis system is developed fast and highly accurate, it can be applied in, and well technically transferred to, the motor manufacturing industry. Once used as quality control testing in automated production lines, it will be able to help save human power and avoid flaw rates that would otherwise be caused by human factors in testing. Moreover, this fast and highly accurate smart motor fault diagnosis system developed herein can also be applied in the monitoring the operating condition of the trains in high speed rail or subway to prevent service problem in mass transit systems caused by deterioration of driving motors.

REFERENCES

[1] A. M. Chao, "Motor fault diagnosis by using fuzzy neural network," Ph.D. dissertation, Dept. Elect. Eng., Chung Yuan Christian Univ., Taoyuan, Taiwan, 2004.

[2] S. C. Peng, "Fault diagnosis by using multiple vibration signals for motor," Ph.D. dissertation, Dept. Elect. Eng., Chung Yuan Christian Univ., Taoyuan, Taiwan, 2004.

[3] M. T. Chang, "Motor fault diagnosis based on extension theory," Ph.D. dissertation, Dept. Elect. Eng., Nat. Chin-Yi Univ. Technol., Taichung, Taiwan, 2007.

[4] T. Han, B.-S. Yang, and J. M. Lee, "A new condition monitoring and fault diagnosis system of induction motors using artificial intelligence algorithms," in *Proc. IEEE Int. Conf. Electr. Mach. Drives*, May 2005, pp. 1967–1974.

[5] F. Pedrayes, C. H. Rojas, M. F. Cabanas, M. G. Melero, G. A. Orcajo, and J. M. Cano, "Application of a dynamic model based on a network of magnetically coupled reluctances to rotor fault diagnosis in induction motors," in *Proc. IEEE Int. Symp. Diagnostics Electr. Mach., Power Electron. Drives*, Sep. 2007, pp. 241–246.
[6] J. Lehtoranta and H. N. Koivo, "Fault diagnosis of induction motors with dynamical neural networks," in *Proc. IEEE Int. Conf. Syst., Man Cybern.*, vol. 3, Oct. 2005, pp. 2979–2984.
[7] Q. He and D.-M. Du, "Fault diagnosis of induction motor using neural networks," in *Proc. Int. Conf. Mach. Learn. Cybern.*, Aug. 2007, pp. 1090–1095.
[8] S. Khomfoi and L. M. Tolbert, "Fault diagnosis system for a multilevel inverter using a principal component neural network," in *Proc. 37th IEEE Power Electron. Spec. Conf.*, Jun. 2006, pp. 1–7.
[9] S. Wu and T. W. S. Chow, "Induction machine fault detection using SOM-based RBF neural networks," *IEEE Trans. Ind. Electron.*, vol. 51, no. 1, pp. 183–194, Feb. 2004.
[10] S. Khomfoi and L. M. Tolbert, "Fault diagnostic system for a multilevel inverter using a neural network," in *Proc. 31st Annu. Conf. IEEE Ind. Electron. Soc.*, Nov. 2005, pp. 1455–1460.
[11] I. E. Alguindigue, A. Loskiewicz-Buczak, and R. E. Uhrig, "Monitoring and diagnosis of rolling element bearings using artificial neural networks," *IEEE Trans. Ind. Electron.*, vol. 40, no. 2, pp. 209–217, Apr. 1993.
[12] H.-I. Son, T.-J. Kim, D.-W. Kang, and D.-S. Hyun, "Fault diagnosis and neutral point voltage control when the 3-level inverter faults occur," in *Proc. IEEE 35th Annu. Power Electron. Spec. Conf.*, vol. 6, Jun. 2004, pp. 4558–4563.
[13] H. Guesmi, S. B. Salem, and K. Bacha, "Smart wireless sensor networks for online faults diagnosis in induction machine," *Comput. Elect. Eng.*, vol. 41, pp. 226–239, Jan. 2015.
[14] P. Konar and P. Chattopadhyay, "Multi-class fault diagnosis of induction motor using Hilbert and Wavelet transform," *Appl. Soft Comput.*, vol. 30, pp. 341–352, May 2015.
[15] P. Konar, J. Sil, and P. Chattopadhyay, "Knowledge extraction using data mining for multi-class fault diagnosis of induction motor," *Neurocomputing*, vol. 166, pp. 14–25, Oct. 2015.
[16] J. Pons-Llinares, J. A. Antonino-Daviu, M. Riera-Guasp, S. B. Lee, T.-J. Kang, and C. Yang, "Advanced induction motor rotor fault diagnosis via continuous and discrete time–frequency tools," *IEEE Trans. Ind. Electron.*, vol. 62, no. 3, pp. 1791–1802, Mar. 2015.
[17] A. Soualhi, G. Clerc, and H. Razik, "Detection and diagnosis of faults in induction motor using an improved artificial ant clustering technique," *IEEE Trans. Ind. Electron.*, vol. 60, no. 9, pp. 4053–4062, Sep. 2013.
[18] O. Duque-Perez, L.-A. Garcia-Escudero, D. Morinigo-Sotelo, P.-E. Gardel, and M. Perez-Alonso, "Analysis of fault signatures for the diagnosis of induction motors fed by voltage source inverters using ANOVA and additive models," *Electr. Power Syst. Res.*, vol. 121, pp. 1–13, Apr. 2015.
[19] L. Saidi, F. Fnaiech, H. Henao, G. A. Capolino, and G. Cirrincione, "Diagnosis of broken-bars fault in induction machines using higher order spectral analysis," *ISA Trans.*, vol. 52, no. 1, pp. 140–148, Jan. 2013.
[20] V. F. Pires, M. Kadivonga, J. F. Martins, and A. J. Pires, "Motor square current signature analysis for induction motor rotor diagnosis," *Measurement*, vol. 46, no. 2, pp. 942–948, Feb. 2013.
[21] K. N. Gyftakis, D. V. Spyropoulos, J. C. Kappatou, and E. D. Mitronikas, "A novel approach for broken bar fault diagnosis in induction motors through torque monitoring," *IEEE Trans. Energy Convers.*, vol. 28, no. 2, pp. 267–277, Jun. 2013.
[22] M. Pineda-Sanchez, R. Puche-Panadero, M. Riera-Guasp, J. Perez-Cruz, J. Roger-Folch, J. Pons-Llinares, V. Climente-Alarcon, and J. A. Antonino-Daviu, "Application of the teager–kaiser energy operator to the fault diagnosis of induction motors," *IEEE Trans. Energy Convers.*, vol. 28, no. 4, pp. 1036–1044, Dec. 2013.
[23] B. Xu, L. Sun, L. Xu, and G. Xu, "Improvement of the Hilbert method via ESPRIT for detecting rotor fault in induction motors at low slip," *IEEE Trans. Energy Convers.*, vol. 28, no. 1, pp. 225–233, Mar. 2013.
[24] K.-H. Chao, M.-S. Yang, and C.-P. Hung, "Islanding detection method of a photovoltaic power generation system based on a CMAC neural network," *Energies*, vol. 6, no. 8, pp. 4152–4169, Aug. 2013.
[25] C.-P. Hung and M.-H. Wang, "Diagnosis of incipient faults in power transformers using CMAC neural network approach," *Electr. Power Syst. Res.*, vol. 71, no. 3, pp. 235–244, Nov. 2004.
[26] J. S. Albus, "A new approach to manipulator control: The cerebeller model articulation controller," *J. Dyn. Syst., Meas., Control*, vol. 97, no. 3, pp. 220–227, Sep. 1975.
[27] W. Cai and C. Yang, *Extension Engineering Methods*. Beijing, China: Science Press, 1997.
[28] C. P. Hung, H. J. Su, and S. L. Yang, "Melancholia diagnosis based on GDS evaluation and meridian energy measurement using CMAC neural network approach," *WSEAS Trans. Inf. Sci. Appl.*, vol. 6, no. 3, pp. 500–509, Mar. 2009.
[29] Y. Wong and A. Sideris, "Learning convergence in the cerebellar model articulation controller," *IEEE Trans. Neural Netw.*, vol. 3, no. 1, pp. 115–121, Jan. 1992.
[30] C. C. Feng and S. J. Huang, "Machine vibration and high-speed spindle test," G-Tech Instrum. Inc., Hsinchu, Taiwan, Tech. Rep., 2005.

PI-YUN CHEN received the Ph.D. degree from the Graduate School of Engineering Science and Technology, National Yunlin University of Science and Technology, in 2011. She is currently an Associate Professor with the Department of Electrical Engineering, National Chin-Yi University of Technology, Taiwan. Her current research interests include fuzzy systems and advanced control systems.

KUEI-HSIANG CHAO received the B.S. degree in electrical engineering from the National Taiwan Institute of Technology, Taipei, Taiwan, in 1988, and the M.S. and Ph.D. degrees in electrical engineering from National Tsing Hua University, Hsinchu, Taiwan, in 1990 and 2000, respectively. He is currently a Professor with the National Chin-Yi University of Technology, Taichung, Taiwan. His current research interests include computer-based control systems, applications of control theory, renewable energy, and power electronics. He is a Life Member of the Solar Energy and New Energy Association.

YU-CHENG TSENG received the B.S. degree in electrical engineering from the National Chin-Yi University of Technology, Taichung, Taiwan, in 2013, where he is currently pursuing the master's degree. His research interests include motor fault diagnosis, motor control, energy storage, and the application of cerebellar model articulation controller.